

RIS-aided Cooperative FD-SWIPT-NOMA Outage Performance in Nakagami- m Channels

Wilson de Souza Junior and Taufik Abrão

Abstract

In this work, we investigate reconfigurable intelligent surfaces (RIS)-assisted cooperative non-orthogonal multiple access (C-NOMA) consisting of two paired users, where the phases of RIS are configured to boost the cell-center device. The cell-center device is designated to act as a full-duplex (FD) relay to assist the cell-edge device. The cell-center device does not use its battery energy to cooperate but harvests energy using simultaneous wireless information power transfer (SWIPT). A more practical non-linear energy harvesting model is considered. Expressions for outage probability (OP) and ergodic rate (ER) are devised, assuming that all users' links undergo Nakagami- m channel fading. We first approximate the harvested power as Gamma random variables via the moments matching technique. This allows us to derive analytical OP/ER expressions that are simple to compute yet accurate for a wide range of RIS passive elements configurations, energy harvesting (EH) coefficients, and residual self-interference (SI) levels, being extensively validated by numerical simulations. The OP expressions reveal how paramount is to mitigate the SI in the FD relay mode since for reasonable values of residual SI coefficient ($\omega \geq -20\text{dB}$), it is notable its detrimental effect on the system performance. Also, numerical results reveal that by increasing the number of RIS elements can be much more beneficial to the cooperative system than the non-cooperative system.

Index Terms

RIS, NOMA, Outage Probability, Ergodic Rate, Cooperative, SWIPT, Nakagami- m , Self-Interference, Energy Harvest.

This work was supported in part by the CAPES (Financial Code 001) and National Council for Scientific and Technological Development (CNPq) of Brazil under Grant 310681/2019-7.

W. Junior and T. Abrão are with the Department of Electrical Engineering (DEEL). State University of Londrina (UEL). Po.Box 10.011, CEP:86057-970, Londrina, PR, Brazil. Email: wilsoonjr98@gmail.com; taufik@uel.br

I. INTRODUCTION

Among several highly important services addressed by the fifth generation (5G) communication systems, and also predicted to be present in wireless communications systems beyond 5G, massive machine-type communication (mMTC) is a use case scenario widely targeted due to the exponential increasing of devices interconnected inside a network. Since wireless networks have become denser, one of the challenges is to support heavy traffic. In recent studies in the literature, it has been proven that *non-orthogonal multiple access* (NOMA) can be superior to the multiple access schemes as deployed in the past generations of cellular networks, including frequency division multiple access (FDMA), time division multiple access (TDMA), and code division multiple access (CDMA), which possibly may not be able to scale to meet such new 5G use case demands. NOMA can be regarded as an interesting candidate to overcome such challenges, once NOMA technology allows multiple users to transmit in the same resource block (RB), which can lead to higher spectral efficiency (SE) and energy efficiency (EE), than the usual *orthogonal multiple access* (OMA). By adopting NOMA, successive interference cancellation (SIC) is paramount to distinguish the respective user's signal, being essential for NOMA to work suitably.

In a cellular system, the connectivity of the cell-edge devices is often affected due to their geographical position; hence, to improve fairness, the cell-edge devices need to be allocated a large number of resources, which can harm the QoS of the cell-center users. Cooperative communications can be a potential solution for this issue once it can improve the cell-edge users' data rate and enhance the network's fairness. The integration of NOMA and cooperative user relaying has attracted significant attention mainly due to the natural matching of both techniques since the cell-edge user information can be known to the cell-center users [1]. Such a scenario is critical since device-to-device (D2D) communication is one of the key technologies for the next generations of communication systems [2], [3]. Cooperative communications can be performed under two distinct modes: half-duplex (HD) and full-duplex (FD). The HD mode is known for sub-dividing the transmission time block, which can degrade the SE, while the FD mode can be performed simultaneously at the cost of *self-interference* (SI) aggregation. Notably, the cooperative NOMA (C-NOMA) system was first proposed and studied in [4], where the cell-center users are selected as relays to guarantee the QoS of the cell-edge users; thus, the OP and the diversity order are performance metrics of interest. In addition, [5], [6] investigated the

performance of FD/HD cooperative NOMA systems.

Although performance gains could be achieved with cooperative communications, the deployment of such technology can be detrimental to the battery lifetime of the devices since inevitably, it drains the battery energy of the cell-center users. In this sense, *simultaneous wireless information and power transfer* (SWIPT) is a promising and sustainable technology that can be useful to address this issue while enabling the implementation of the internet of things (IoT), since IoT devices are usually energy-limited for relay cooperation. Moreover, the SWIPT technique allows the devices to harvest energy from the ambient radio-frequency (RF) sources and reuse it to cooperate with the cell-edge users. SWIPT also can be implemented in two ways, *power-splitting* (PS) and *time-switching* (TS) [7]. The PS-SWIPT protocol splits the received signal power from the base station (BS) into two parts, one for *information decoding* (ID), and the other for *energy harvesting* (EH) purposes. On the other hand, the TS-SWIPT protocol necessarily splits the time slots to perform the ID and EH processes separately. [8]–[11] investigate the system performance of the SWIPT-assisted C-NOMA system over FD/HD mode, carrying out extensive analyses on the OP/ER. Moreover, [12] proposes an alternative optimization-based algorithm to jointly optimize the power allocation, power splitting, receiver filter and transmit beamforming in a SWIPT-assisted C-NOMA system.

Recently, *reflecting intelligent surface* (RIS) has attracted remarkable research attention due to its capability of changing and customizing the wireless propagation environment, hence supporting high system throughput and being useful in indoor/outdoor scenarios where dense obstacles arise. The RIS is composed of scattering elements, *i.e.*, artificial meta-material structures composed of adaptive composite material layers, which can reflect incident electromagnetic waves and can be configured to increase the signal level in a specific direction for a priority user, and it is calling attention mainly due to its features: the capacity to be sustainable, low-power consumption, enhancing communications metrics, facility of implementation and installation, compatibility and low cost. In [13], the RIS-assisted non-C-NOMA system has been analytically validated in terms of OP considering two-user scenarios; indeed, RIS-aided communication can substantially improve the system OP. In [14], the impact of the BS-user direct link on the system performance is evaluated by comparing the RIS-aided system with the relay-aided system. Furthermore, the performance of RIS-aided non-C-NOMA system has been analyzed in [15] from the perspective of imperfect SIC effects. On the other hand, in [16], the authors assess the impact of RIS phase shift design on the OP, ER, and bit error probability (BER) through

two phase-shift configurations: random phase, and coherent phase-shifting under Nakagami- m fading. Recently, [17] provides valuable analytical results on the OP for downlink RIS-assisted backscatter communications with NOMA. In [18], the RIS-NOMA system OP under hardware impairments has been analyzed analytically: an accurate closed-form for the OP was developed. Very recently, the end-to-end channel statistics for both weakest and strongest users in a *non*-cooperative RIS-aided NOMA system under Nakagami- m was derived in [19]. In [20], a RIS-aided cooperative NOMA scheme was analyzed from the perspective of power consumption.

A. Motivation and Contributions

To further improve the throughput, reliability, and fairness of mobile devices, the integration of different technologies such as NOMA, cooperative system with SWIPT and RIS is very promising; furthermore, there are few works in the literature dealing with RIS-aided C-NOMA SWIPT systems [21]–[23]. A hybrid TS and PW EH relaying for RIS-NOMA system with transmit antenna selection is proposed in [21], while in [23] the authors intended to minimize the transmit power at both the BS and at the user-cooperating relay. Differently, in [22], the authors proposed an algorithm to jointly optimize the beamforming and the power splitting coefficient. However, to the best of our knowledge, so far, no studies have provided a solid investigation on the OP/ER performance of RIS-aided NOMA systems, the integration of RIS-aided cooperative communications assuming non-linear energy harvesting model operating under generalized Nakagami- m fading channels.

Motivated by the aforementioned facts, in this work we aim to investigate the *potential benefits of combining RIS, NOMA, and cooperative communications with SWIPT and non-linear EH circuits*. Herein, in order to suitably unveil the system OP performance, we focus on a two-user scenario with perfect SIC and perfect knowing channel state information (CSI) at the BS¹.

In light of the above motivations and challenges, the main *contributions* of this work are threefold and can be summarized as follows:

- We analyze a cooperative NOMA system scenario under Nakagami- m fading channels, combined with the SWIPT technique adopting a non-linear energy harvesting model, where the cell-center device cooperates with the cell-edge device without harming itself in terms

¹Most complex, intricate scenarios, and performance metrics such as secrecy outage, sum rate, etc, are out of the scope of this work and will be treated in future works.

of battery lifetime. Besides, we investigate the use of RIS aiming to identify its benefits and drawbacks operating under the considered scenario.

- We derive novel general expressions for the OP and upper bound of ER for the analyzed system. Since such expression is parameterized w.r.t. the system and channel parameters, the effect of each parameter can be effectively scanned as a function of the number of RIS elements.
- Comprehensive numerical results simulations for the OP, ER and user rate corroborating the effectiveness and accuracy of the proposed analytical performance expressions.

The adopted methodology allows us to assess analytically the RIS-aided cooperative SWIPT-NOMA performance, which is essential to predict how the system acts in practice.

Notation: $\Gamma(\cdot)$ is the gamma function; $\gamma(\cdot, \cdot)$ is the lower incomplete gamma function; $\Gamma(\cdot, \cdot)$ is the upper incomplete gamma function; $\text{Ei}(\cdot)$ is exponential integral function; $X \sim \mathcal{CN}(\mu, \sigma^2)$ denotes a random variable X following a Complex Normal distribution with mean μ and variance σ^2 ; $X \sim \text{Gamma}(k, \theta)$ denotes a random variable following a Gamma distribution with shape parameter k and scale parameter δ ; $X \sim \text{Exponential}(\lambda)$ denotes a random variable following a Exponential distribution with rate parameter λ ; $X \sim \text{Rayleigh}(\sigma)$ denotes a random variable following a Rayleigh distribution with scale parameter σ ; the magnitude of a complex number z is expressed by $|z|$; $\arg(\cdot)$ denotes the argument of a complex number; $\text{diag}(\cdot)$ denotes the diagonal operator; vectors and matrices are represented by bold-face letters; F_X denotes the cumulative density function (CDF) of X ; f_X denotes the probability density function (PDF); and $\text{Pr}(\cdot)$ expresses probability.

II. SYSTEM MODEL

Let us consider a RIS-assisted C-NOMA downlink where a source (S) equipped with a single antenna simultaneously serves two devices. Let us denote the cell-center device as D_1 , while D_2 is the cell-edge device as represented in Fig. 1. The transmission process is assisted by an N -elements RIS.

The direct link between the source and the devices is assumed to be completely obstructed. The application scenarios for the system model illustrated in Fig. 1 are leveraged with the advent of IoT systems. The adopted setup directly applies to environments where D2D communication can benefit, including offices and residences. Furthermore, there is a vast potential for application in industries and communication/automation between industrial robots.

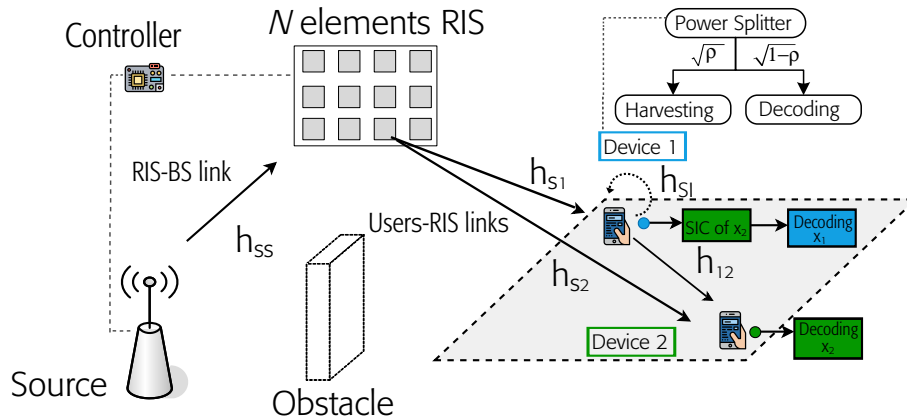


Fig. 1. Downlink C-FD-SWIPT-NOMA system model, consisting of a source (S) and two paired devices, D_1 and D_2 . To improve the performance of D_2 , the device D_1 acts as a full-duplex relay under the self-interference (SI) effect.

To ensure QoS to the system, D_1 can act as a cooperative relay adopting the decode-and-forward (DF) protocol [24], [25]. In order to reach ultra-low latency in the cooperative framework, a primordial feature in the 5G and 6G communication systems, in this work we have assumed that the cooperative device (D_1) is equipped with two antennas, where the first one is responsible for receiving the signal and the other antenna to relaying [26]; hence, the cooperative process (at the user-relay) can occur in an FD mode [1], [10], [12], [27], [28] but subject to self-interference (SI). SI or loop-interference (LI) refers to the signal that is transmitted by the transmitter antenna operating in the FD node and looped back to the receiver antenna at the same node [6].

To do not jeopardize the battery lifetime of D_1 , such a device can take advantage of the SWIPT technique by adopting the PS architecture [11], [29], where a fraction ρ of the received power is utilized to energy harvesting and the remaining fraction $(1 - \rho)$ to perform information decoding. The energy harvested can be fully utilized to relay the rebuilt message version of D_2 .

The RIS operation is encapsulated by its phase shift matrix, which is assumed to be ideally a lossless surface and given as

$$\Phi = \text{diag}(e^{j\phi_1}, e^{j\phi_2}, \dots, e^{j\phi_N}) \quad (1)$$

where $\phi_n \in (0, 2\pi]$ is the phase shift applied to the n -th element of the RIS. We consider that the RIS is programmed by a dedicated controller connected to the S via a high-speed backhaul [30], whose main aim is to update systematically the RIS phases shift at each coherence-time once the phase-shift variables are directly related to the CSI.

We assume that all link channels experience quasi-static flat fading over a coherence time and vary independently from one coherence time to another. The CSI is assumed to be perfectly known at the S . The small-scale channel from S to the RIS is denoted by $\mathbf{h}_{ss} \in \mathbb{C}^N$, while the small-scale channel between the RIS and the ℓ -th device is denoted by $\mathbf{h}_{s\ell} \in \mathbb{C}^N \forall \ell \in \{1, 2\}$. It is assumed that $|\mathbf{h}_{ss}[n]| = |h_{ss,n}|$ and $|\mathbf{h}_{s\ell}[n]| = |h_{s\ell,n}|$ are independent r.v. following Nakagami- m fading, *i.e.*,

$$\begin{aligned} |h_{ss,n}| &\sim \text{Nakagami}(m_{ss}, \Omega_{ss}), \quad \forall n \in \{1, \dots, N\} \\ |h_{s\ell,n}| &\sim \text{Nakagami}(m_{s\ell}, \Omega_{s\ell}), \quad \forall \ell \in \{1, 2\}, \end{aligned} \quad (2)$$

while the phases are uniformly distributed in the $[0, 2\pi]$ range. Hence, the equivalent channel for the ℓ -th device can be written as:

$$h_\ell = \sqrt{\beta_{ss}\beta_{s\ell}} \mathbf{h}_{ss}^H \Theta \mathbf{h}_{s\ell}, \quad (3)$$

where β_{ss} and $\beta_{s\ell}$ are the large-scale fading of $S \rightarrow \text{RIS}$ link and $\text{RIS} \rightarrow D_\ell$ link respectively. Besides, for the $D_1 \rightarrow D_2$ communication link (D2D), the h_{12} follows a complex Gaussian distribution, *i.e.*, $h_{12} \sim \mathcal{CN}(0, \sqrt{\beta_{12}}) \forall n \in \{1, \dots, N\}$, where β_{12} is the path loss of D2D communication.

In this work, we consider the RIS serving the user-relay with a coherent combination; thus, the phases shift of RIS are set to

$$\phi_n = -\angle h_{ss,n} - \angle h_{s1,n}, \quad \forall n = \{1, \dots, N\} \quad (4)$$

Therefore, the cascaded channel can be written as

$$h_\ell = \sqrt{\beta_{ss}\beta_{s\ell}} \mathbf{h}_{ss} \Phi \mathbf{h}_{s\ell}, \quad \forall \ell \in \{1, 2\} \quad (5)$$

with $\mathbf{h}_{ss} \Phi \mathbf{h}_{s1} = \sum_{n=1}^N |h_{ss,n}| |h_{s1,n}|$ being a real-number² and $\mathbf{h}_{ss} \Phi \mathbf{h}_{s2} = \sum_{n=1}^N e^{j\phi_n} h_{ss,n} h_{s2,n}$, a complex number once the phases of RIS appear random for D_2 .

A. Signal Model

In NOMA, S transmits a superimposed signal $x(t)$ which propagates in direction to the devices through the RIS, with $x = \sqrt{\alpha_1}x_1 + \sqrt{\alpha_2}x_2$, where $\alpha_\ell \in (0, 1)$ denotes the power allocation

²Sum of product between two Nakagami- m r.v., since the RIS is programmed to cancel the phase of $h_{ss,n}$ and $h_{s1,n}$

coefficients, with $\alpha_1 + \alpha_2 = 1$, $\alpha_2 > \alpha_1$ and x_ℓ with $\mathbb{E}[|x_\ell|^2] = 1$ is the message of ℓ -th device, $\ell \in \{1, 2\}$.

1) *Device 1*: The observation at the D_1 which will be designated for ID can be written as follows

$$y_1^{\text{ID}}(t) = \underbrace{h_1 \sqrt{P_t(1-\rho)} x(t)}_{\text{Superimposed information}} + \underbrace{h_{SI} \sqrt{P_H} \hat{x}_2(t-\tau)}_{\text{Self-interference}} + \underbrace{n_1(t)}_{\text{noise}}, \quad (6)$$

where $0 \leq \rho \leq 1$ is the received power fraction utilized to energy harvesting (EH factor), P_t is the transmit power and the SI term comes from by adopting the FD mode at the user-relay. In this work, we consider that channel coefficient related to the SI, h_{SI} , undergo a zero mean complex-Normal distribution [8], [9], [31], [32], with power $|h_{SI}|^2 = \omega$. Besides, $\hat{x}_2(t-\tau)$ is the retransmitted and rebuilt message of D_2 by D_1 , τ denotes the processing delay at the user-relay caused by FD mode, which is assumed lower than the coherence time. The additive white Gaussian noise (AWGN) at the D_1 is modeled as $n_1 \sim \mathcal{CN}(0, \sigma_1^2)$.

2) *Device 2*: The observation at the D_2 can be written as follows

$$y_2(t) = \underbrace{h_1 \sqrt{P_t} x(t)}_{\text{Superimposed information}} + \underbrace{h_{12} \sqrt{P_H} \hat{x}_2(t-\tau)}_{\text{Cooperative transmission}} + \underbrace{n_2(t)}_{\text{noise}}, \quad (7)$$

where n_2 is the AWGN at the D_2 .

Non-Linear EH Model. For the EH process, we employ a practical non-linear model [33]; thus, the power deployed in the relaying step at D_1 (P_H) can be expressed as:

$$P_H(P_{in}) = \frac{P_{th} \left(\frac{1}{1+e^{-a(\rho P_{in}-b)}} - \frac{1}{1+e^{ab}} \right)}{1 - \frac{1}{1+e^{ab}}}, \quad (8)$$

where P_{th} is the threshold harvested power in saturation, a and b are constants related to the EH circuits as capacitance, resistance, and diode turn-on voltage. The adopted non-linear EH model from [33] closely matches experimental/practical EH circuit results for both the low (μW) and high ($m\text{W}$) wireless power harvested regime. The RF input power in the EH circuit at D_1 is defined as:

$$P_{in} = P_t |h_1|^2. \quad (9)$$

B. Signal-Interference-to-Noise-Ratio

D_1 receives a superimposed message y_1 from the $S \rightarrow \text{RIS} \rightarrow D_1$, so, according to NOMA the message of D_2 is detected first, and the corresponding signal-to-interference-plus-noise (SINR) is given by

$$\text{SINR}_{D_1}^{x_2} = \frac{|h_1|^2(1-\rho)P_t\alpha_2}{|h_1|^2(1-\rho)P_t\alpha_1 + |h_{SI}|^2P_H + \sigma^2}, \quad (10)$$

where we consider without loss of generalization that $\sigma_1^2 = \sigma_2^2 = \sigma^2$. After message x_2 is detected, it is eliminated from the received signal (6) by performing the SIC process³, thus, the SINR in D_1 for detecting x_1 is given by

$$\text{SINR}_{D_1}^{x_1} = \frac{|h_1|^2(1-\rho)P_t\alpha_1}{|h_{SI}|^2P_H + \sigma^2}. \quad (11)$$

At D_2 , the received SINR to detect x_2 from $S \rightarrow \text{RIS} \rightarrow D_2$ link, and the received SNR to detect x_2 from $D_1 \rightarrow D_2$ link are respectively expressed as

$$\text{SINR}_{D_2,S}^{x_2} = \frac{|h_2|^2P_t\alpha_2}{|h_2|^2P_t\alpha_1 + \sigma^2}, \quad (12)$$

and

$$\text{SNR}_{D_2,D_1}^{x_2} = \frac{P_H|h_{12}|^2}{\sigma^2}. \quad (13)$$

By adopting the maximum ratio combining (MRC) rule, the overall SINR in D_2 is equivalent to the sum of SINR from $S \rightarrow \text{RIS} \rightarrow D_2$ link and SNR from $D_1 \rightarrow D_2$ link, which can be expressed as [12], [32], [34]

$$\begin{aligned} \text{SINR}_{D_2}^{x_2} &= \text{SINR}_{D_2,S}^{x_2} + \text{SNR}_{D_2,D_1}^{x_2} \\ &= \frac{|h_2|^2P_t\alpha_2}{|h_2|^2P_t\alpha_1 + \sigma^2} + \frac{P_H|h_{12}|^2}{\sigma^2}. \end{aligned} \quad (14)$$

III. STATISTICS OF CHANNEL AND HARVESTED POWER

Our goal is to obtain new expressions that characterize the OP and ER for both devices in the RIS-aided C-NOMA-SWIPT. For that reason, in the following two-subsection we characterize statistically the cascaded channel for both devices as well as the harvested power in D_1 respectively.

³Here we consider that the SIC process is performed perfectly, *i.e.*, we do not take into account an eventual residual error from this process.

A. Statistical Channel Characterization

Before proceeding to the OP derivation, it is paramount to characterize the channel statistically. Let us denote $X_1 = \sum_{n=1}^N |h_{ss,n}| |h_{s1,n}|$ and $X_2 = \left| \sum_{n=1}^N e^{j\phi_n} h_{ss,n} h_{s2,n} \right|$. According to Lemma 2 of [35], the distribution of X_1 and X_2 , can be approximated as

$$X_1 \stackrel{\text{approx}}{\sim} \text{Gamma} \left(N \frac{\mu_{ss}^2 \mu_{s1}^2}{1 - \mu_{ss}^2 \mu_{s1}^2}, \frac{1 - \mu_{ss}^2 \mu_{s1}^2}{\mu_{ss} \mu_{s1}} \right), \quad (15)$$

$$X_2 \stackrel{\text{approx}}{\sim} \text{Rayleigh} \left(\sqrt{\frac{N}{2}} \right), \quad (16)$$

where μ_{ss} and μ_{s1} are the mean of a Nakagami- m r.v. given as [36, Table 5.2]

$$\mu_{ss} = \frac{\Gamma(m_{ss} + 1/2)}{\Gamma(m_{ss})} \sqrt{\frac{\Omega_{ss}}{m_{ss}}}, \quad \mu_{s1} = \frac{\Gamma(m_{s1} + 1/2)}{\Gamma(m_{s1})} \sqrt{\frac{\Omega_{s1}}{m_{s1}}}. \quad (17)$$

Proceeding, Lemma 1 of [35] states that the distribution of X_1^2 and X_2^2 , can be approximated respectively as

$$X_1^2 \stackrel{\text{approx}}{\sim} \text{Gamma}(k_1, \theta_1), \quad (18)$$

$$X_2^2 \stackrel{\text{approx}}{\sim} \text{Exponential}(N), \quad (19)$$

where

$$k_1 = \frac{\left(\mu_{X_1}^{(2)} \right)^2}{\mu_{X_1}^{(4)} - \left(\mu_{X_1}^{(2)} \right)^2}, \quad \theta_1 = \frac{\mu_{X_1}^{(4)} - \left(\mu_{X_1}^{(2)} \right)^2}{\mu_{X_1}^{(2)}}, \quad (20)$$

with $\mu_{X_1}^{(m)}$ being the m -th moment of a Gamma r.v. given as

$$\mu_{X_1}^{(m)} = \frac{\left(\frac{1 - \mu_{ss}^2 \mu_{s1}^2}{\mu_{ss} \mu_{s1}} \right)^m \Gamma \left(N \frac{\mu_{ss}^2 \mu_{s1}^2}{1 - \mu_{ss}^2 \mu_{s1}^2} + m \right)}{\Gamma \left(N \frac{\mu_{ss}^2 \mu_{s1}^2}{1 - \mu_{ss}^2 \mu_{s1}^2} \right)}, \quad (21)$$

thus, the PDF and CDF of X_1^2 and X_2^2 can be written respectively as

$$f_{X_1^2}(x) = \frac{x^{k_1-1} e^{-\frac{x}{\theta_1}}}{\Gamma(k_1) \theta_1^{k_1}}, \quad f_{X_2^2}(x) = \frac{1}{N} e^{-\frac{x}{N}}, \quad (22)$$

$$F_{X_1^2}(x) = \frac{\gamma \left(k_1, \frac{x}{\theta_1} \right)}{\Gamma(k_1)}, \quad F_{X_2^2}(x) = 1 - e^{-\frac{x}{N}}. \quad (23)$$

B. Statistical Harvested Power Characterization

We also should analyze the distribution of the harvested power in D_1 when D_1 intends to act as a relay ($\rho \neq 0$), thus for this purpose, the following lemma is conceived.

Lemma 1. Let $\zeta = aP_t\rho\beta_{ss}\beta_{s1}\theta_1$, the distribution of P_H in Eq. (8) can be approximated as a Gamma r.v. $P_H \stackrel{\text{approx}}{\sim} \text{Gamma}\left(k_{P_H}, \frac{P_{th}}{1+e^{ab}}\theta_{P_H}\right)$ for $\zeta \ll 1$ where k_{P_H} and θ_{P_H} are given respectively by

$$k_{P_H} = \frac{\left(\frac{(1+e^{ab})^{k_1-1}}{(1+e^{ab}(1-\zeta))^{k_1}} - \frac{1}{1+e^{ab}}\right)^2}{\frac{(1+e^{ab})^{k_1-2}}{(1+e^{ab}(1-\zeta))^{k_1}} - \frac{(1+e^{ab})^{2k_1-2}}{(1+e^{ab}(1-\zeta))^{2k_1}}}, \quad (24)$$

$$\theta_{P_H} = \frac{\frac{(1+e^{ab})^{k_1-2}}{(1+e^{ab}(1-\zeta))^{k_1}} - \frac{(1+e^{ab})^{2k_1-2}}{(1+e^{ab}(1-\zeta))^{2k_1}}}{\frac{(1+e^{ab})^{k_1-1}}{(1+e^{ab}(1-\zeta))^{k_1}} - \frac{1}{1+e^{ab}}}}. \quad (25)$$

Proof. The proof is available in Appendix A ■

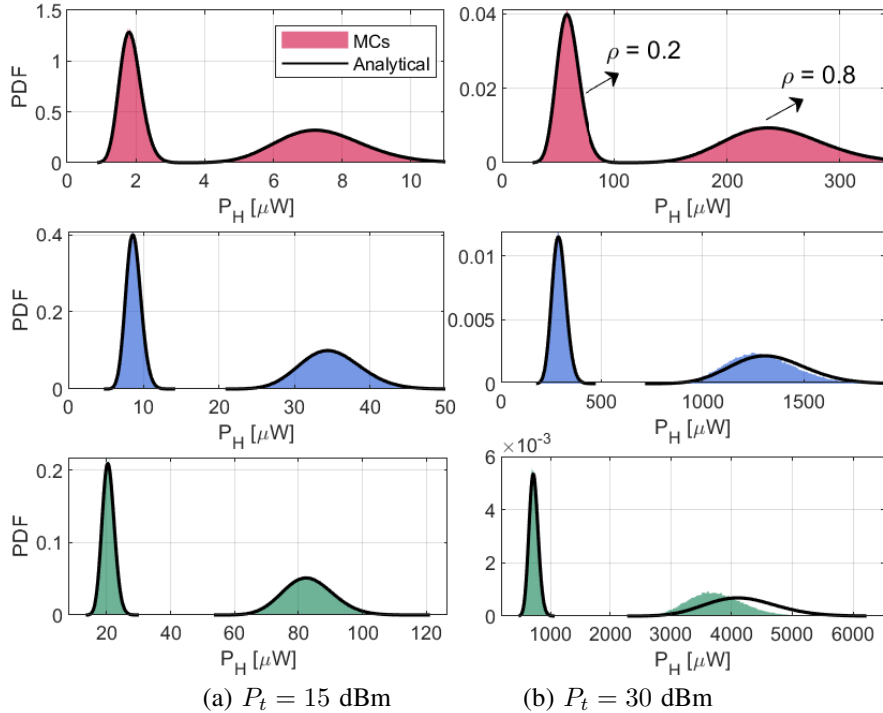


Fig. 2. PDF of the harvested power P_H for $N = 30$ (red color), $N = 65$ (blue color) and $N = 100$ (green color), with $\rho = 0.2$ (left slope) and $\rho = 0.8$ (right slope). Another parameters are in Table I.

Remark 1. The mean harvested power can be computed as

$$\begin{aligned}\bar{P}_H &= k_{P_H} \theta_{P_H} \\ &= \frac{P_{th}}{1 - \frac{1}{1+e^{ab}}} \left(\frac{(1 + e^{ab})^{k_1-1}}{(1 + e^{ab}(1 - \zeta))^{k_1}} - \frac{1}{1 + e^{ab}} \right).\end{aligned}\quad (26)$$

IV. SYSTEM PERFORMANCE ANALYSIS

In order to explore the advantages in RIS-aided C-SWIPT-NOMA scenarios, in this section new expressions for the OP and SE of D_1 and D_2 in the RIS-aided C-SWIPT-NOMA system considering generalized Nakagami- m fading channels and non-linear energy harvesting model are presented, where we consider that target SINRs are determined by the devices' QoS requirements. The OP metric is paramount to evaluate the reliability of the transmission in the 5G and 6G systems, specially in the URLLC use mode.

A. Device 1 Outage Probability

Particularly, the outage behavior for D_1 occurs since D_1 cannot detect effectively x_2 and consequently its own message or when x_2 is detected successfully but an error occurs to decode x_1 , *i.e.*, the outage occurs except for the case that both D_2 and itself message are decoded successfully. Mathematically it can be formulated by

$$P_{\text{out}}^{D_1} = 1 - \Pr(\text{SINR}_{D_1}^{x_2} \geq \gamma_{th2}, \text{SINR}_{D_1}^{x_1} \geq \gamma_{th}), \quad (27)$$

where $\gamma_{th2} = 2^{R_2} - 1$ and $\gamma_{th} = 2^{R_1} - 1$, with R_1 and R_2 being the target rates of the D_1 and D_2 , respectively. The following theorem provides the OP of D_1 for RIS-aided C-SWIPT-NOMA system.

Theorem 1. Let $\xi_1 = \frac{\gamma_{th}}{P_t(1-\rho)\alpha_1}$ and $\xi_2 = \frac{\gamma_{th2}}{P_t(1-\rho)(\alpha_2 - \alpha_1\gamma_{th2})}$, if $\alpha_2 < \alpha_1\gamma_{th2}$ or $\frac{k_1\theta_1\beta_{ss}\beta_{s1}}{\xi_1} < \omega k_{P_H} \theta_{P_H}$, $P_{\text{out}}^{D_1} = 1$, otherwise the closed-form expression for the OP of D_1 under Nakagami- m fading is given by (28) when $\rho = 0$ or $\omega = 0$, or by (29) at top of the next page when $\rho \neq 0$ and $\omega \neq 0$

$$P_{\text{out}}^{D_1} = \begin{cases} \frac{\gamma \left(k_1, \frac{\xi_1 \sigma^2}{\theta_1 \beta_{ss} \beta_{s1}} \right)}{\Gamma(k_1)}, & \text{if } \xi_1 > \xi_2 \\ \frac{\gamma \left(k_1, \frac{\xi_2 \sigma^2}{\theta_1 \beta_{ss} \beta_{s1}} \right)}{\Gamma(k_1)}, & \text{otherwise.} \end{cases} \quad (28)$$

$$P_{\text{out}}^{D_1} \approx \begin{cases} \frac{\gamma\left(k_1, \frac{\xi_1 \sigma^2}{\theta_1 \beta_{ss} \beta_{s1}}\right)}{\Gamma(k_1)} + \frac{e^{\frac{\sigma^2}{\omega k_{P_H} \theta_{P_H}}} \xi_1 \omega k_{P_H} \theta_{P_H}}{\Gamma(k_1)} \frac{\Gamma\left(k_1, \xi_1 \sigma^2 \left(\frac{1}{\theta_1 \beta_{ss} \beta_{s1}} + \frac{1}{\xi_1 \omega k_{P_H} \theta_{P_H}}\right)\right)}{(\xi_1 \omega k_{P_H} \theta_{P_H} + \theta_1 \beta_{ss} \beta_{s1})^{k_1}} & \xi_1 > \xi_2 \\ \frac{\gamma\left(k_1, \frac{\xi_2 \sigma^2}{\theta_1 \beta_{ss} \beta_{s1}}\right)}{\Gamma(k_1)} + \frac{e^{\frac{\sigma^2}{\omega k_{P_H} \theta_{P_H}}} \xi_2 \omega k_{P_H} \theta_{P_H}}{\Gamma(k_1)} \frac{\Gamma\left(k_1, \xi_2 \sigma^2 \left(\frac{1}{\theta_1 \beta_{ss} \beta_{s1}} + \frac{1}{\xi_2 \omega k_{P_H} \theta_{P_H}}\right)\right)}{(\xi_2 \omega k_{P_H} \theta_{P_H} + \theta_1 \beta_{ss} \beta_{s1})^{k_1}} & \xi_1 < \xi_2 \end{cases} \quad (29)$$

Proof. The proof is available in Appendix B. ■

B. Device 2 Outage Probability

The outage behavior for the D_2 can occur in two distinct ways: 1) D_1 detects effectively the D_2 ' message however the sum of the SINRs after MRC in D_2 is lower than the SINR of threshold or 2) D_1 cannot detect effectively the D_2 ' message and the SINR becoming of the $S \rightarrow \text{RIS} \rightarrow D_2$ is lower than the SINR of threshold. Therefore, the OP of D_2 can be formulated as

$$P_{\text{out}}^{D_2} = \Pr(\text{SINR}_{D_1}^{x_2} < \gamma_{th2}, \text{SINR}_{D_2, S}^{x_2} < \gamma_{th2}) + \Pr(\text{SINR}_{D_1}^{x_2} \geq \gamma_{th2}, \text{SINR}_{D_2}^{x_2} < \gamma_{th2}). \quad (30)$$

Theorem 2. Let us define $I = 1 - e^{-\frac{\sigma^2 \gamma_{th2}}{k_{P_H} \theta_{P_H} \beta_{12}}} - e^{-\frac{-\sigma^2 \gamma_{th2}}{P_t \beta_{ss} \beta_{s2} N(\alpha_2 - \alpha_1 \gamma_{th2})}} \frac{\left(e^{\frac{\sigma^2 \gamma_{th2}}{P_t \beta_{ss} \beta_{s2} N(\alpha_2 - \alpha_1 \gamma_{th2})} - \frac{\gamma_{th2} \sigma^2}{\beta_{12} k_{P_H} \theta_{P_H}}} - 1 \right)}{\frac{\beta_{12} k_{P_H} \theta_{P_H}}{P_t \beta_{ss} \beta_{s2} N(\alpha_2 - \alpha_1 \gamma_{th2})} - 1}$, and let the following variable given as $\chi = \frac{\gamma\left(k_1, \frac{\xi_2 \sigma^2}{\theta_1 \beta_{ss} \beta_{s1}}\right)}{\Gamma(k_1)} + \frac{e^{\frac{\sigma^2}{\omega k_{P_H} \theta_{P_H}}} \xi_2 \omega k_{P_H} \theta_{P_H}}{\Gamma(k_1)} \frac{\Gamma\left(k_1, \xi_2 \sigma^2 \left(\frac{1}{\theta_1 \beta_{ss} \beta_{s1}} + \frac{1}{\xi_2 \omega k_{P_H} \theta_{P_H}}\right)\right)}{(\xi_2 \omega k_{P_H} \theta_{P_H} + \theta_1 \beta_{ss} \beta_{s1})^{k_1}}$, for the case when $\alpha_2 < \alpha_1 \gamma_{th2}$, then $P_{\text{out}}^{U_2} = 1$, otherwise, then the closed-form expression for the OP of D_2 under Nakagami- m fading is given by

$$P_{\text{out}}^{U_2} \approx \begin{cases} 1 - e^{-\frac{-\sigma^2 \gamma_{th2}}{P_t \beta_{ss} \beta_{s2} N(\alpha_2 - \alpha_1 \gamma_{th2})}}, & \text{if } \rho = 0 \\ I + \chi \left(1 - I - e^{-\frac{-\sigma^2 \gamma_{th2}}{P_t \beta_{ss} \beta_{s2} N(\alpha_2 - \alpha_1 \gamma_{th2})}} \right) & \text{if } \rho \neq 0, \end{cases} \quad (31)$$

Proof. Please refer to Appendix C. ■

C. Device 1 Ergodic Rate

In this subsection, to understand better the RIS-aided C-SWIPT-NOMA system with a non-linear EH model, we proposed an upper bound for the ER of D_1 .

Theorem 3. *Assuming the D_1 can successfully detect D_2 and itself message, then the upper bound spectral efficiency for D_1 under Nakagami- m fading can be calculated as*

$$R_1 \leq \log_2 \left(1 - \frac{\beta_{ss}\beta_{s1}k_1\theta_1(1-\rho)P_t\alpha_1 e^{-\frac{\sigma^2}{\omega k_{P_H}\theta_{P_H}}} \text{Ei} \left(-\frac{\sigma^2}{\omega k_{P_H}\theta_{P_H}} \right)}{\omega k_{P_H}\theta_{P_H}} \right) \quad (32)$$

Proof. The ER of D_1 can be expressed through $\mathbb{E}[R_1] = \mathbb{E}[\log_2(1 + \text{SINR}_{D_1}^{x_1})]$. Therefore, by utilizing the Jensen' inequality, we can obtain a upper bound for rate of D_1 as $\mathbb{E}[R_1] \leq \log_2 \left(1 + \mathbb{E} \left[\frac{|h_1|^2(1-\rho)P_t\alpha_1}{|h_{SI}|^2 P_H + \sigma^2} \right] \right)$, where

$$\begin{aligned} \mathbb{E} \left[\frac{1}{|h_{SI}|^2 P_H + \sigma^2} \right] &= \frac{1}{\omega k_{P_H}\theta_{P_H}} \int_0^\infty \frac{e^{-\frac{x}{\omega k_{P_H}\theta_{P_H}}}}{x + \sigma^2} dx \\ &= \frac{-e^{-\frac{\sigma^2}{\omega k_{P_H}\theta_{P_H}}} \text{Ei} \left(-\frac{\sigma^2}{\omega k_{P_H}\theta_{P_H}} \right)}{\omega k_{P_H}\theta_{P_H}}, \end{aligned} \quad (33)$$

where [37, 3.352.4] is utilized. ■

D. Device 2 Ergodic Rate

An upper bound for the ER of D_2 is proposed in the following theorem.

Theorem 4. *Assuming the D_2 decoded successfully the message of x_2 from $S \rightarrow \text{RIS} \rightarrow D_2$ as well as the rebuilt message \hat{x}_2 from the cooperative link (since D_1 decoded successfully x_2 in order to relay it), the upper bound for ER of D_2 is given as*

Proof. Realizing the same step as done in Appendix, we obtain Eq. (34), where

$$R_2 \leq \log_2 \left(1 + \frac{\alpha_2 \sigma^2 e^{\frac{\sigma^2}{N\beta_{ss}\beta_{s2}P_t\alpha_1}}}{N\beta_{ss}\beta_{s2}P_t\alpha_1^2} \Gamma \left(-1, \frac{\sigma^2}{N\beta_{ss}\beta_{s2}P_t\alpha_1} \right) + \frac{k_{P_H}\theta_{P_H}\beta_{12}}{\sigma^2} \right) \quad (34)$$

$$\begin{aligned} \mathbb{E} \left[\frac{|h_2|^2 P_t \alpha_2}{|h_2|^2 P_t \alpha_1 + \sigma^2} \right] &= \int_0^\infty \frac{|h_2|^2 P_t \alpha_2}{|h_2|^2 P_t \alpha_1 + \sigma^2} f_{|h_2|^2} d|h_2|^2 \\ &\stackrel{(i)}{=} \frac{\alpha_2}{\alpha_1 N} \int_0^\infty \frac{x e^{-\frac{x}{N}}}{x + \frac{\sigma^2}{\beta_{ss}\beta_{s2}P_t\alpha_1}} dx \\ &= \frac{\alpha_2 \sigma^2}{N\beta_{ss}\beta_{s2}P_t\alpha_1^2} e^{\frac{\sigma^2}{N\beta_{ss}\beta_{s2}P_t\alpha_1}} \\ &\quad \times \Gamma \left(-1, \frac{\sigma^2}{N\beta_{ss}\beta_{s2}P_t\alpha_1} \right), \end{aligned} \quad (35)$$

utilizing (22) and [37, 3.383.10] is utilized in (i). ■

Corollary 1. When $P_t \rightarrow \infty$, the ER of D_2 , R_2^∞ can be computed as

$$= \begin{cases} \log_2 \left(1 + \frac{\alpha_2}{\alpha_1} \right), & \rho = 0 \\ \log_2 \left(1 + \frac{\alpha_2}{\alpha_1} \right) - \frac{e^{\frac{\sigma^2(1+\frac{\alpha_2}{\alpha_1})}{P_{th}\beta_{12}}} \text{Ei} \left(-\frac{\sigma^2(1+\frac{\alpha_2}{\alpha_1})}{P_{th}\beta_{12}} \right)}{\ln(2)}, & \rho \neq 0 \end{cases} \quad (36)$$

Proof. When $\rho = 0$, it reaches the conventional NOMA case and can be solved trivially, otherwise, when $\rho \neq 0$, and $P_t \rightarrow \infty$, due to the non-linear EH model, $P_H = P_{th}$, therefore the ER of D_2 is given as

$$R_2^\infty = \mathbb{E} \left[\log_2 \left(1 + \frac{\alpha_2}{\alpha_1} + \frac{P_{th}|h_{12}|^2}{\sigma^2} \right) \right], \quad (37)$$

hence

$$\begin{aligned}
R_2^\infty &= \int_0^\infty \log_2 \left(1 + \frac{\alpha_2}{\alpha_1} + \frac{P_{th}\beta_{12}x}{\sigma^2} \right) e^{-x} dx \\
&\stackrel{(i)}{=} \frac{\sigma^2}{P_{th}\beta_{12} \ln(2)} \int_0^\infty \ln \left(1 + \frac{\alpha_2}{\alpha_1} + x \right) e^{-\frac{\sigma^2 x}{P_{th}\beta_{12}}} \\
&= \log_2 \left(1 + \frac{\alpha_2}{\alpha_1} \right) - \frac{e^{-\frac{\sigma^2(1+\frac{\alpha_2}{\alpha_1})}{P_{th}\beta_{12}}}}{\ln(2)} \text{Ei} \left(-\frac{\sigma^2 \left(1 + \frac{\alpha_2}{\alpha_1} \right)}{P_{th}\beta_{12}} \right),
\end{aligned} \tag{38}$$

where in (i) [38, 4.337.1] is utilized. ■

V. SIMULATION RESULTS

In this section, we aim to confirm through Monte-Carlo simulations (MCs) the accuracy of our previous mathematical analysis and illustrate the achievable enhanced performance of the RIS-aided cooperative FD-SWIPT-NOMA system. The simulation results are averaged over 10^6 realizations. Unless stated otherwise, the parameter values adopted in this section are presented in Table I. In the following numerical results, the Monte-Carlo simulation curves are labeled as "MCs", and the derived analytical expression-based curves are labeled as "Analytical". We use dashed lines to represent the D_1 performance, while D_2 is represented by solid lines. In addition, color red, blue and green, denotes the simulations for $N = 30, 65$, and 100 RIS elements, respectively.

A. Ergodic Rate vs Transmit Power

Fig. 3 depicts the ER of D_1 and D_2 vs P_t for three values of $N = \{30; 65; 100\}$ RIS-elements. Firstly we can notice that the derived upper bound expressions given by Eq. (32) and Eq. (34) respectively are very tight when $\rho = 0$; furthermore, when $\rho = 0.2$, the upper bound is especially tight for low values of P_t , for any N , as P_t increases, the ratio between the ER and the derived upper bound decreases. We also can note that after a specific value of P_t , the derived equations become inaccurate. This can be justified by the adoption made in Appendix A, where $aP_t\rho\beta_{ss}\beta_{s1}\theta_1 \ll 1$. We separate the accurate region (I) (denoted by low power regime and green color) and the inaccurate region (II) (high power regime red color). Notice that as stated, the regions vary according to N , ρ , and P_t (since β_{ss} , β_{s1} and a are fixed values), when

TABLE I
ADOPTED SIMULATION PARAMETERS.

Parameter	Value
RIS-aided Cooperative FD-SWIPT-NOMA system	
Transmit power	$P_t = [0, 50]$ [dBm]
Noise power	$\sigma^2 = -96$ dBm/Hz
Bandwidth	$B = 1$ MHz
# RIS elements	$N = \{30; 65; 100\}$
Power Allocation coefficients	$\alpha_1 = 0.9, \alpha_2 = 0.1$
Target Rate	$R_1 = 1.5, R_2 = 0.5$ [bits/s]
Residual Self-Interference	$h_{SI} \sim \mathcal{CN}(0, \omega)$, with $\omega = -[\infty; 30; 15]$ [dB]
Non-Linear Energy Harvesting Parameters	
EH coefficient	$\rho \in [0, 1]$
EH model constants	$a = 150; b = 0.014$ [39], [40]
Max. RF (harvested) power	$P_{th} = 24$ [mW] [39], [40]
Channel Parameters	
Channel Model (S -RIS/RIS- D_s)	Nakagami- m
Shape Parameter S -RIS	$m_{ss} = 3.5$
Shape Parameter RIS- D_s	$m_{s1} = 2, m_{s2} = 1$
Spread Parameter	$\Omega_{s1} = \Omega_{s2} = 1$
Channel Model (D2D)	$h_{12} \sim \mathcal{CN}(0, \beta_{12})$
Path losses	$\beta_{ss} = -30$ dB, $\beta_{s1} = -30$ dB $\beta_{s2} = -40$ dB, $\beta_{12} = -15$ dB

$N = 30$, the region (II) occurs for $P_t > 49$ dBm, as well as $P_t > 43$ and $P_t > 39$ for $N = 65$ and $N = 100$ respectively.

Concerning the RIS-aided C-SWIPT-NOMA system performance, we can see that when $\rho = 0$, this configuration represents the conventional NOMA system, thus, for any value of N , D_1 naturally reaches higher rates than D_2 , furthermore, D_2 reaches a maximum rate when $P_t \rightarrow \infty$, given by Eq. (36). For the cooperative scenario, $\rho = 0.2$, we can see that rate of D_1 increases initially till reaching a maximum value then it decreases and afterward increases again. This behavior can be explained by the non-linear EH model, once P_t increases, D_1 can harvest a higher amount of power, and when it reaches the saturation P_{th} , the interference in the denominator of Eq. (11) is limited, hence by increasing the transmit power, the rate of D_1 increases again. In addition, we can confirm that the value of maximum rate reached by D_2 is not dependent of N , *i.e.*, the RIS cannot contribute to increase the rate of D_2 when $P_t \rightarrow \infty$, however it can be achieved with lower power when N increases. It is confirmed in Eq. (36), where we can see that R_2^∞ can vary in function of $\alpha_1, \alpha_2, P_{th}, \beta_{12}$ and σ^2 .

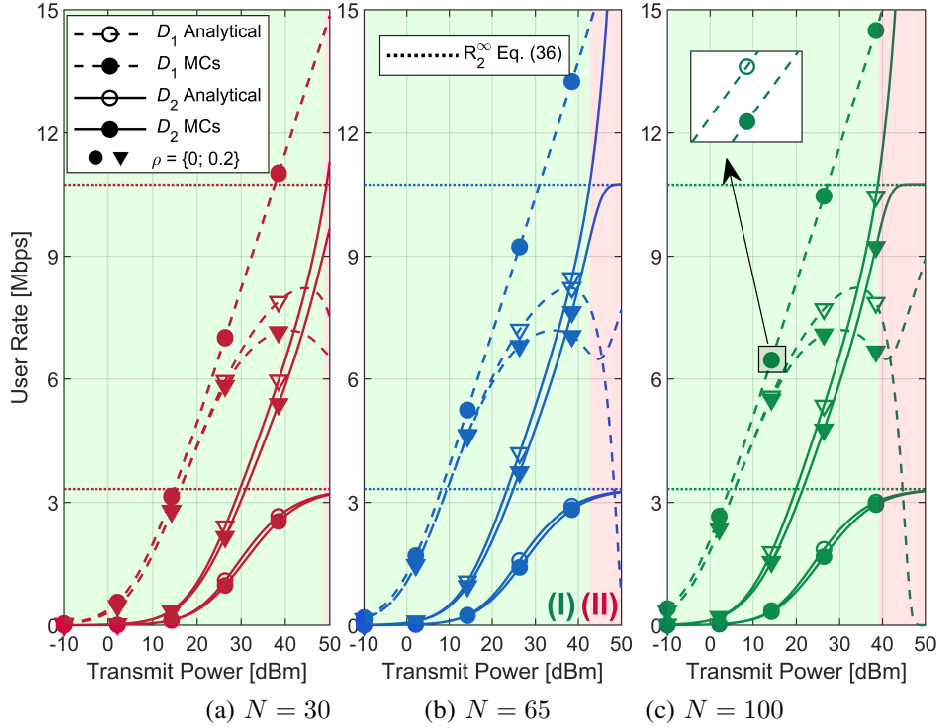


Fig. 3. ER vs P_t for three values of number of elements of RIS $N = \{30; 65; 100\}$ in RIS-aided C-SWIPT-NOMA system, with $\rho = \{0; 0.2\}$.

B. Harvested Power vs Transmit Power

Fig. 4 illustrate the behaviour of the harvested power P_H parameterized in the transmitted power P_t for the MCs and the analytical derived result. We firstly notice that Eq. (26) is very accurate for low and middle values of P_t , i.e., $P_t \leq 30$ dBm. Besides, in this region we can see that the harvested power increases linearly with the transmitted power. We also can see that for higher values of P_t , the P_H saturates in P_{th} , independently of value of N . This is expected since a non-linear EH model is adopted.

C. Outage Probability vs Transmit Power

Fig. 5 depicts the OP performance vs the transmit power in the node S . Firstly, one can infer that the derived equations (29) and (31) are very accurate for the values of ρ and P_t from -10 to 50 dBm till the order of 10^{-5} for the OP. Besides, one can infer that in the cooperative scenario the reliability of device D_2 increases considerably, mainly when N assumes high values; in contrast, due to power drainage to operate as a relay, the device D_1 has a loss of performance, as also confirmed in Fig. 3 and 6, considering $\rho = 0.2$ and 0.5 , respectively. Herein, to understand the

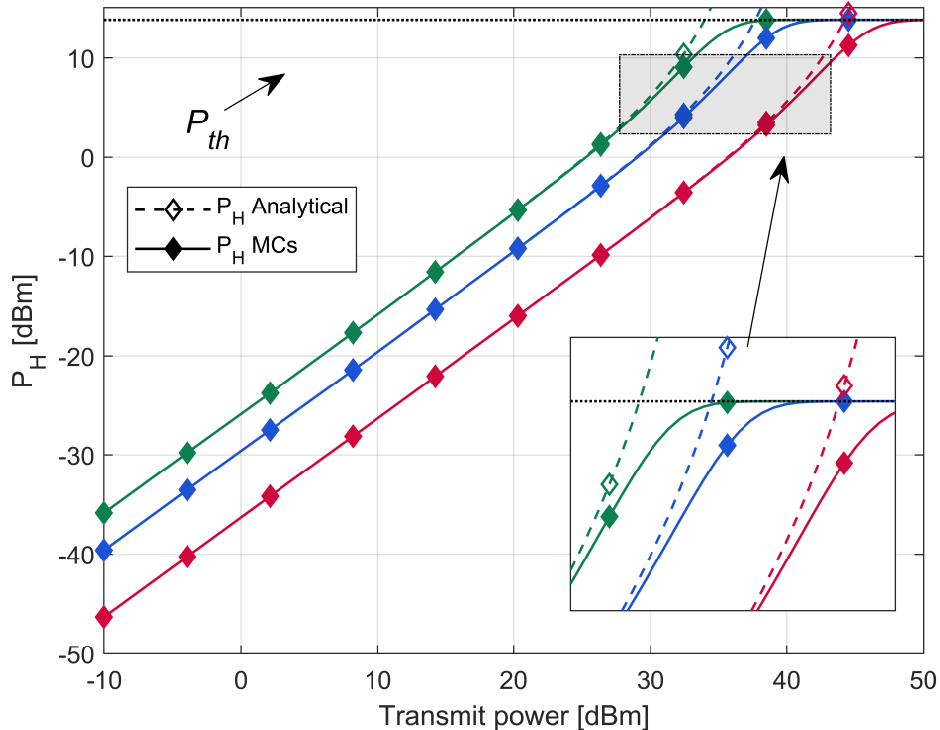


Fig. 4. P_H vs P_t with non-linear EH model, where $\rho = 0.8$. Here we adopt $N = \{30; 65; 100\}$ as red, blue and green color respectively.

potential of the studied RIS-aided cooperative FD-SWIPT-NOMA system, we consider the ideal case where $\omega = 0$, *i.e.* there is no residual self-interference cancellation in the SIC stage. We can see that although D_1 operates in worst conditions when $\rho = 0.2$, its OP performance degradation is marginal when related to the OP gain obtained by D_2 , indicating that the cooperative scenario can be very interesting for D_1 if there is no residual self-interference and mainly for D_2 due to the remarkable improvement in the OP performance gain attained. Moreover, one can see that by increasing the value of N , the OP performance loss in D_1 can not be mitigated, while the gain of performance of D_2 becomes lower.

D. Ergodic Rate vs RIS elements

Fig. 6 illustrates the impact of the number of elements of RIS on the device rate (D_1 and D_2) when $P_t = 15$ dBm for $\rho = 0$ and $\rho = 0.5$. Notice that our derived upper bounds given by Eqs. (32) and (34) can represent the behavior of the rate of both devices. Also, one can see that for the non-cooperative scenario ($\rho = 0$), naturally, D_1 can achieve a substantial performance gain over D_2 ; furthermore, when N increases, the enhanced performance is further highlighted in D_1

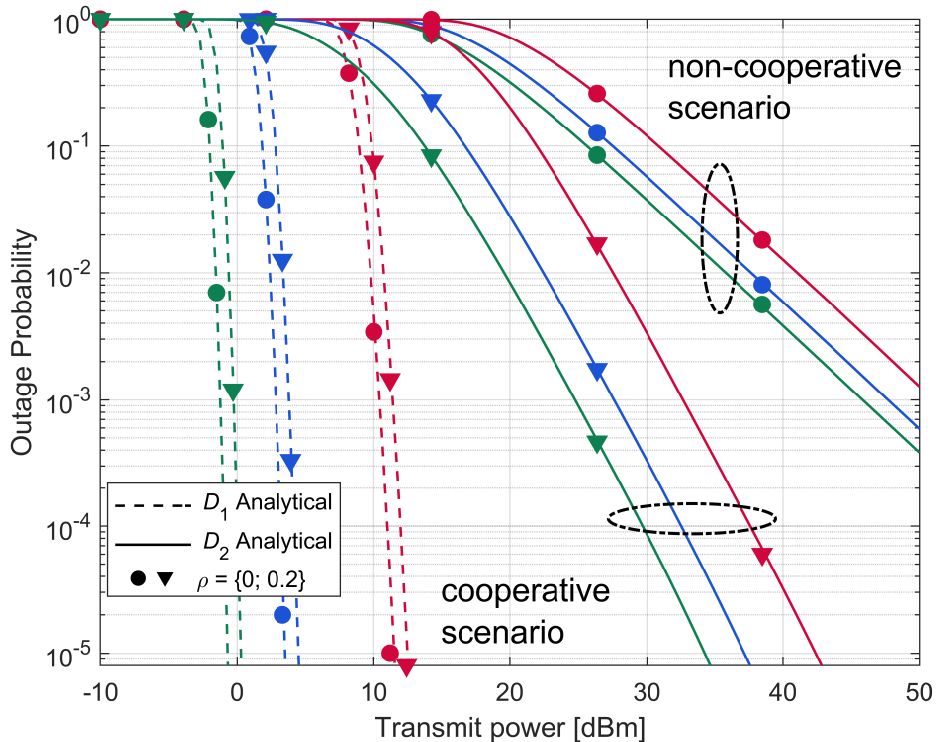


Fig. 5. OP vs P_t for $N = \{30, 65, 100\}$ (red, blue and green, respectively), and $\rho = \{0; 0.2\}$, where we consider the ideal case $\omega = 0$, in order to see how is the best performance of the system with the considered parameters.

than D_2 , it is due to the RIS being configured to boost D_1 (coherent phase shift matrix for D_1), while the rate of D_2 increases marginally (from ≈ 0.15 to ≈ 0.4) when N becomes higher (once that random phase shift matrix is set). On the other hand, in the cooperative scenarios ($\rho = 0.5$), one can notice that the D_1 rates are lower than in the former case, which is expected since D_1 drains energy to operate as a relay. Besides, notably, the impact of the ω in the ER of D_1 is very harmful if we assume high values of ω and its impact is highlighted for large values of N . However, in such a scenario, D_2 can achieve higher rates, and now, it effectively increases as N increases, *e.g.*, the rate of D_2 increases from ≈ 0.7 bits/s to 2.5 bits/s, obtaining a very interesting gain in terms of ER that was not possible in the non-cooperative case. Effectively, RIS-aided systems can contribute to the cooperative system in order to provide better conditions for the cell-edge devices and consequently provide better fairness indexes for RIS-aided cooperative FD-SWIPT-NOMA communication systems.

Next, to understand the impact of the residual self-interference on the OP, in Fig. 7 we studied how the performance of D_1 can be affected when the SIC operation is degraded by increasing the residual SI factor ω ; herein we have evaluated the OP degradation for $\omega \in \{-\infty, -20, -15\}$

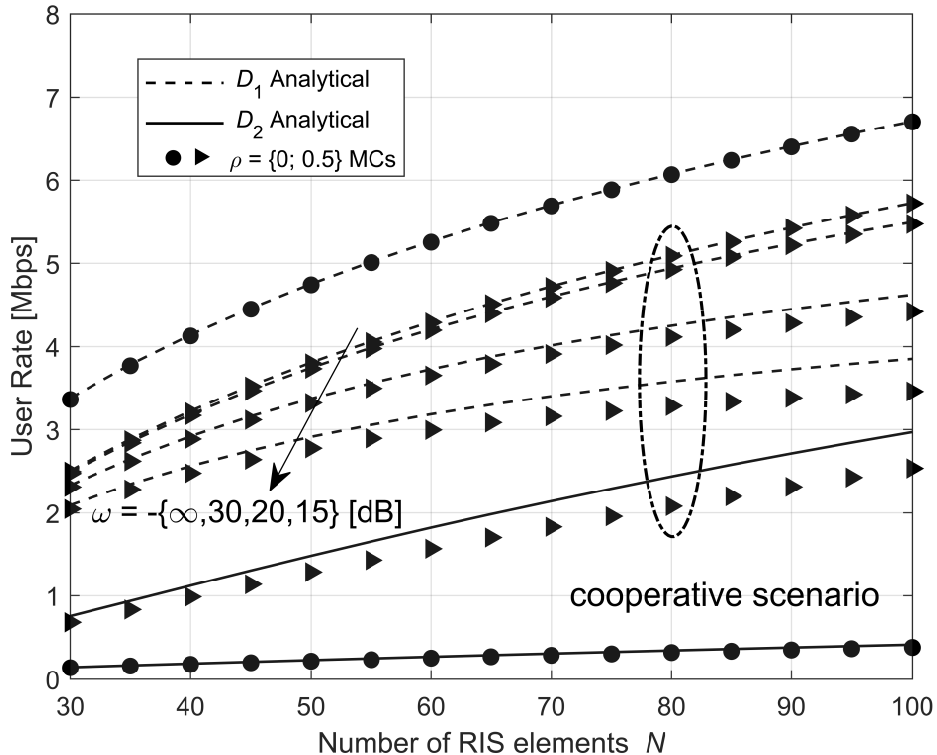


Fig. 6. ER vs N for cooperative and non-cooperative scenario $\rho = \{0; 0.5\}$, $P_t = 15$ dBm and $\omega = \{-45, -30, -15\}$ dB.

dB and considering $N = 100$ RIS antenna-elements. As a benchmark, we consider the linear EH model with an efficiency of $\eta = 0.8$ to understand its impacts and differences when adopting a more realistic non-linear EH model. One can see that naturally, D_1 achieves better performance when $\omega = 0$; hence, as ω increases, its performance is severely degraded for both linear and non-linear EH models. Furthermore, it is notable that the linear EH model has an additional negative impact on the OP performance of D_1 , for any value of ω . The reason is that the linear EH model can harvest much more power than the non-linear model, leading to higher interference. Finally, we also can see that the linear and non-linear EH model reveal different asymptotic operational behaviors, *i.e.*, when $P_t \rightarrow \infty$, the linear EH model saturates in an OP floor where this behavior already has been reported in the literature [5], [10]. In contrast, one can see that the asymptotic behavior of the non-linear EH model reveals a continuous increase in the OP of D_1 till to reach a maximum (when P_H saturates), and then it is expected to start decreasing again according to the behavior illustrated in Fig. 3. It is paramount to understand that the main reason to this behavior is that the linear model provides false considerations about the EH operation, *i.e.*, when $P_t \rightarrow \infty$, $P_H \rightarrow \infty$, which is not physically possible, in contrast, for the non-linear EH model,

when $P_t \rightarrow \infty$, $P_H \rightarrow P_{th}$; hence, for higher values of power, it is expected that $P_{out}^{D_1}$ become 0.

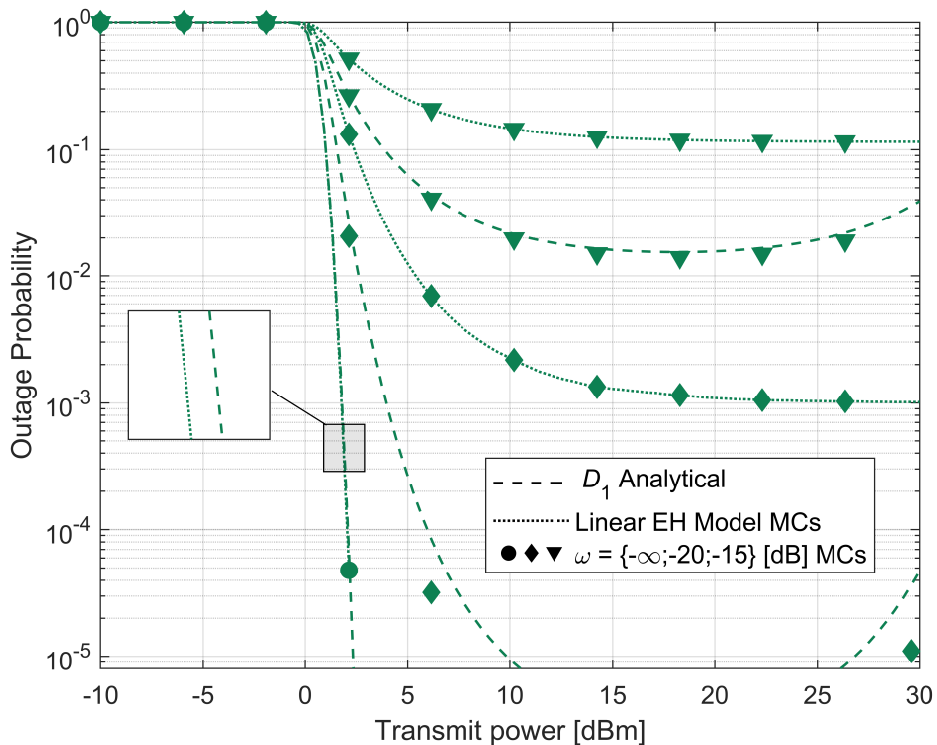


Fig. 7. OP vs P_t with $N = 100$ and $\rho = 0.5$, for non-linear EH model and linear EH model.

E. Outage Probability vs Energy Harvest Coefficient

To gain further insights, in Fig. 8 we plot the OP of both devices against the EH coefficient in the range $\rho \in [0.0; 1.0]$, considering two different transmission power $P_t = 15$ and $P_t = 30$ [dBm], with $\omega = \{-5, -10, -15\}$ dB and $N = 100$ RIS elements. Firstly, one can notice the significant reliability improvement on D_2 by changing the ρ value, from low to intermediate values, considering both values of P_t . Besides, one can see how it is important to reduce the residual self-interference, in order to D_1 to be able to cooperate. We notice that when the system is not well designed to remove the self-interference, the D_2 performance can become worst, *e.g.*, when SI factor is very high, *i.e.*, $\omega = -5$ dB, D_2 performance becomes worst if $\rho > 0.65$, $\rho > 0.45$ for $P_t = 15$ and $P_t = 30$ dBm respectively. It is justified due to the interference increasing over D_1 , which impacts the decoding of D_2 ' message, and thus, D_1 can not operate as a relay. Also, notice that when ω assumes lower values, D_1 can drain and cooperate with high values of ρ , while its own OP performance is just marginally impacted.

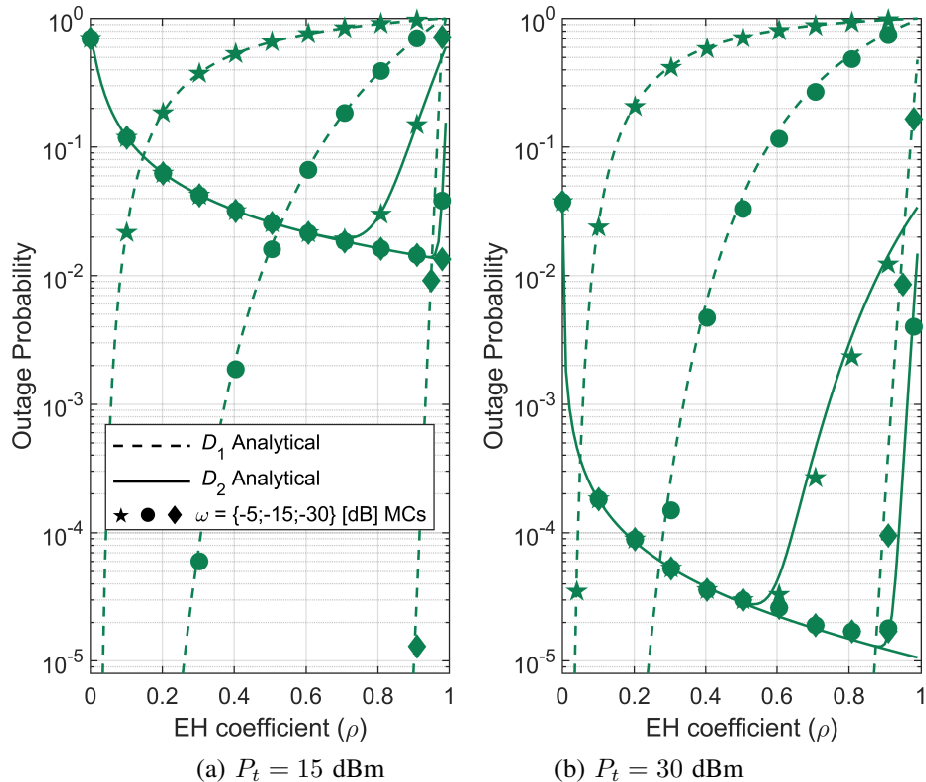


Fig. 8. OP vs ρ for $N = 100$ under (a) $P_t = 15$ [dBm]; (b) $P_t = 30$ [dBm]. Impact of SI factor $\omega = \{-5, -15, -30\}$ [dB] on the OP of D_1 and D_2 .

F. Outage Probability vs Threshold Power

Fig. 9 shows the impact of P_{th} on the OP performance of both devices. When the D_1 has a higher capacity to harvest power (higher P_{th} values), the performance of D_2 is further improved. On the other hand, the self-interference also is increased and consequently worst its own performance. Also, the negative impact of the SI on the performance is notable, confirming how it is paramount to reduce ω in order to does not jeopardize the D_1 performance, mainly when P_{th} assume high values.

VI. CONCLUSIONS

This work has investigated the downlink communication reliability and throughput of both the cell-center and the cell-edge device in RIS-aided cooperative SWIPT-NOMA system operating under Nakagami- m fading; the cell-center device leverages of SWIPT technique equipped with a non-linear EH model to act as a FD-DF relay for assisting the cell-edge device. It was shown that under certain conditions, the harvested power in the cell-center device can be approximated as

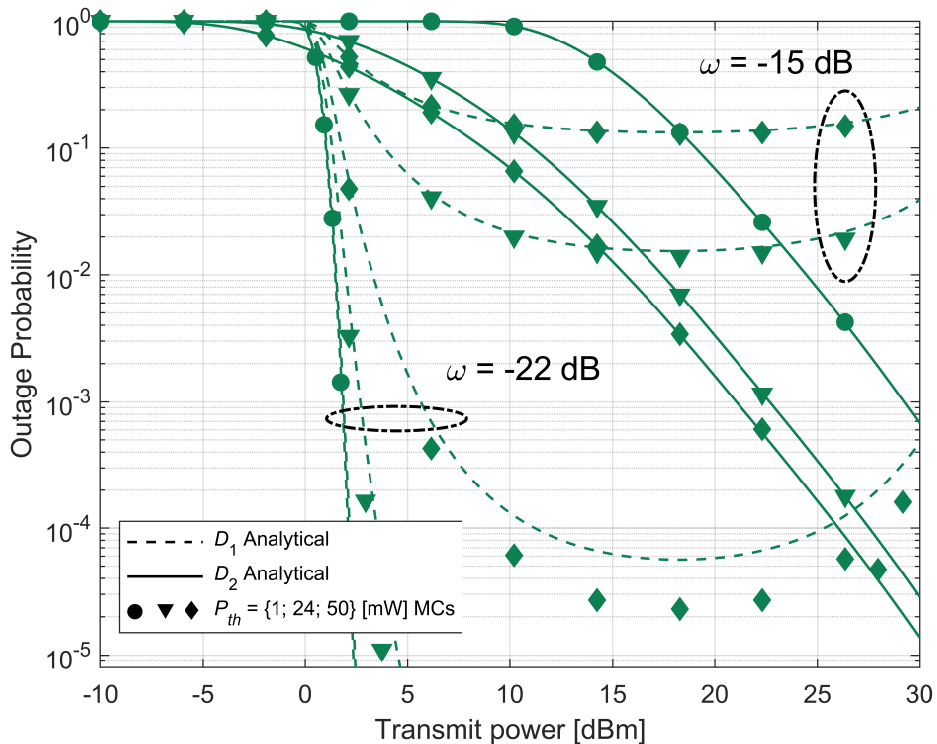


Fig. 9. OP vs P_t for $N = 100$, $\rho = 0.5$ and $\omega = \{-22; -15\}$ [dB]. Herein, $P_{th} = \{1; 25; 50\}$ mW.

a Gamma random variable, allowing flexible modeling of the system. We have derived tractable closed-form expressions for the performance of both types of users, including: **a)** upper bound for ER of a cell-center/edge devices; **b)** tight expression for OP of both devices; and **c)** maximum rate that the cell-edge user can attain in the cooperative mode. In addition, we assessed the impact of the RIS dimension on both metrics adopted. Also, it is demonstrated that the RIS can effectively improve the data rate of the cell-edge device when the cell-center device is cooperating. Besides, we show how paramount is to mitigate the residual self-interference till when N assumes large values. Simulation results validate the correctness and the effectiveness of the developed theoretical analysis while demonstrate the advantages of the analyzed RIS-aided cooperative SWIPT-NOMA system over the non-cooperative RIS-aided system.

APPENDIX A
PROOF OF LEMMA 1

Let us define $Y = \frac{1}{1+e^{-a(\rho P_{in}-b)}}$, thus we can write the first moment of Y as

$$\mathbb{E}[Y] = \mathbb{E} \left[\frac{1}{1+e^{-a(\rho P_{in}-b)}} \right] = \int_0^\infty \frac{f_{|h_1|^2}(x)}{1+e^{-a(\rho P_t \beta_{ss} \beta_{s1} x - b)}} dx. \quad (39)$$

To the best of the authors' knowledge, the integral in Eq. (39) does not admit closed-form expression, here we will utilize the following approximation $e^{-aP_t \rho \beta_{ss} \beta_{s1} x} \approx 1 - aP_t \rho \beta_{ss} \beta_{s1} x$. This approximation is reasonable for lower values of transmit power (P_t) and RIS elements (N) since $a\rho\beta_{ss}\beta_{s1} \ll 1$, once the product of path losses naturally assume low values, thus substituting (22) in (39), we obtain

$$\begin{aligned} \mathbb{E}[Y] &\approx \frac{1}{\Gamma(k_1)\theta_1^{k_1}(1+e^{ab})} \int_0^\infty x^{k_1-1} e^{-x\left(\frac{1}{\theta_1} - \frac{e^{ab} a P_t \rho \beta_{ss} \beta_{s1}}{1+e^{ab}}\right)} dx \\ &\approx \frac{(1+e^{ab})^{k_1-1}}{(1+e^{ab}(1-aP_t\rho\beta_{ss}\beta_{s1}\theta_1))^{k_1}}, \end{aligned} \quad (40)$$

where [37, 3.381.4] is utilized. Realizing same step above, similarly, the second moment of Y can be given by

$$\mathbb{E}[Y^2] \approx \frac{(1+e^{ab})^{k_1-2}}{(1+e^{ab}(1-2aP_t\rho\beta_{ss}\beta_{s1}\theta_1))^{k_1}}. \quad (41)$$

Therefore utilizing the M.M. technique, the shape and scale parameter of P_H in Eq. (8) can be evaluated as follows

$$k_{P_H} = \frac{\left(\mathbb{E}[Y] - \frac{1}{1+e^{ab}}\right)^2}{\mathbb{E}[Y^2] - \mathbb{E}[Y]^2}, \quad (42)$$

$$\theta_{P_H} = \frac{\mathbb{E}[Y^2] - \mathbb{E}[Y]^2}{\mathbb{E}[Y] - \frac{1}{1+e^{ab}}}. \quad (43)$$

Plugging (40) and (41) in (42) and (43); (24) (25) are obtained and this completes the proof.

APPENDIX B
PROOF OF THEOREM 1

After some manipulations, Eq. (27) can be written as

$$P_{\text{out}}^{D_1} = \Pr\left(X_1^2 < \max\left\{\frac{\xi_1(|h_{SI}|^2 P_H + \sigma^2)}{\beta_{ss}\beta_{s1}}, \frac{\xi_2(|h_{SI}|^2 P_H + \sigma^2)}{\beta_{ss}\beta_{s1}}\right\}\right), \quad (44)$$

where $\xi_2 = \frac{\gamma_{th2}}{P_t(1-\rho)(\alpha_2 - \alpha_1\gamma_{th2})}$ and $\xi_1 = \frac{\gamma_{th}}{P_t(1-\rho)\alpha_1}$. Clearly, when $\rho = 0$ or $\omega = 0$, we have that

$$P_{\text{out}}^{D_1} = \begin{cases} \frac{\gamma\left(k_1, \frac{\xi_1\sigma^2}{\theta_1\beta_{ss}\beta_{s1}}\right)}{\Gamma(k_1)}, & \text{if } \xi_1 > \xi_2 \\ \frac{\gamma\left(k_1, \frac{\xi_2\sigma^2}{\theta_1\beta_{ss}\beta_{s1}}\right)}{\Gamma(k_1)}, & \text{otherwise.} \end{cases} \quad (45)$$

When we have $\rho \neq 0$ and $\omega \neq 0$, (44) should be further analyzed. Firstly, we should notice that according to Appendix A, P_H is a Gamma r.v. with shape and scale parameters given by k_{PH} and θ_{PH} respectively. Thus (44) can be written as

$$P_{\text{out}}^{D_1} = 1 - \Pr\left(\underbrace{\xi_\ell |h_{SI}|^2 P_H}_V - \underbrace{X_1^2 \beta_{ss} \beta_{s1}}_Z < -\xi_\ell \sigma^2\right), \quad (46)$$

let us define $V = \xi_\ell |h_{SI}|^2 P_H$ and $Z = X_1^2 \beta_{ss} \beta_{s1}$. Here, we proposed to approximate V as a exponential r.v., *i.e.*, $V \stackrel{\text{approx}}{\sim} \text{Exponential}(\xi_\ell \omega k_{PH} \theta_{PH})$. Since Z is the product of X_1 with a constant, we have $Z \sim \text{Gamma}(k_1, \theta_1 \beta_{ss} \beta_{s1})$, hence, (46) can be written as

$$\begin{aligned} P_{\text{out}}^{D_1} &= 1 - \int_{\xi_\ell \sigma^2}^{\infty} F_V(z - \xi_\ell \sigma^2) f_Z(z) dz \\ &= 1 - \int_{\xi_\ell \sigma^2}^{\infty} f_Z(z) dz + e^{\frac{\sigma^2}{\omega k_{PH} \theta_{PH}}} \int_{\xi_\ell \sigma^2}^{\infty} e^{-\frac{x}{\xi_1 \omega k_{PH} \theta_{PH}}} f_Z(z) dz \\ &= \frac{\gamma\left(k_1, \frac{\xi_\ell \sigma^2}{\theta_1 \beta_{ss} \beta_{s1}}\right)}{\Gamma(k_1)} + \frac{e^{\frac{\sigma^2}{\omega k_{PH} \theta_{PH}}} \xi_1 \omega k_{PH} \theta_{PH}}{\Gamma(k_1)} \\ &\quad \times \frac{\Gamma\left(k_1, \xi_1 \sigma^2 \left(\frac{1}{\theta_1 \beta_{ss} \beta_{s1}} + \frac{1}{\xi_1 \omega k_{PH} \theta_{PH}}\right)\right)}{(\xi_1 \omega k_{PH} \theta_{PH} + \theta_1 \beta_{ss} \beta_{s1})^{k_1}}, \end{aligned} \quad (47)$$

where we utilized the exponential CDF and [37, 3.381.9] to solve (47).

APPENDIX C
PROOF OF THEOREM 2

To derive the OP of D_2 it is reasonable to separate it in two cases, *i.e.*, when the D_1 does not operate as relay ($\rho = 0$), and when the D_1 operates as a relay ($\rho \neq 0$).

I) $\rho = 0$ (D_1 does not act as a relay)

After some manipulations, we can written (30) as

$$P_{\text{out}}^{D_2} = \Pr \left(|h_2|^2 < \frac{\sigma^2 \gamma_{th2}}{P_t(\alpha_2 - \alpha_1 \gamma_{th2})} \right), \quad (48)$$

utilizing the CDF of exponential r.v., we obtain the following

$$P_{\text{out}}^{D_2} = 1 - e^{-\frac{1}{\beta_{ss}\beta_{s2}N} \left(\frac{\sigma^2 \gamma_{th2}}{P_t(\alpha_2 - \alpha_1 \gamma_{th2})} \right)}. \quad (49)$$

II) $\rho \neq 0$ (D_1 operates as a relay)

After some manipulations, we can written (30) as

$$\begin{aligned} P_{\text{out}}^{D_2} &= \Pr \left(|h_1|^2 < \xi_2(\omega P_H + \sigma^2), |h_2|^2 < \frac{\sigma^2 \gamma_{th2}}{P_t(\alpha_2 - \alpha_1 \gamma_{th2})} \right) \\ &+ \Pr \left(|h_1|^2 \geq \xi_2(\omega P_H + \sigma^2), \right. \\ &\left. \frac{P_t |h_2|^2}{\sigma^2} < \frac{\gamma_{th2} - \frac{P_H}{\sigma^2} |h_{1,2}|^2}{\alpha_2 - \alpha_1 \gamma_{th2} + \alpha_1 \frac{P_H}{\sigma^2} |h_{1,2}|^2} \right). \end{aligned} \quad (50)$$

Let us define $\overline{W} = \frac{P_H}{\sigma^2} |h_{1,2}|^2$, since P_H assume lower values than $|h_{1,2}|^2$, we approximate \overline{W} as exponential r.v., $\overline{W} \sim \exp \left(\frac{\theta_{P_H} k_{P_H} \beta_{12}}{\sigma^2} \right)$, hence

$$\begin{aligned} &\Pr \left(\frac{P_t |h_2|^2}{\sigma^2} < \frac{\gamma_{th2} - \overline{W}}{\alpha_2 - \alpha_1 \gamma_{th2} + \alpha_1 \overline{W}} \right) \\ &= \int_0^{\gamma_{th2}} \int_0^{\frac{\gamma_{th2}-y}{\alpha_2 - \alpha_1 \gamma_{th2} + \alpha_1 y}} f_{\frac{P_t |h_2|^2}{\sigma^2}}(x) f_{\overline{W}}(y) dx dy \\ &= \underbrace{F_{\overline{W}}(\gamma_{th2}) - \int_0^{\gamma_{th2}} \sigma^2 e^{\left(\frac{-\sigma^2}{P_t \beta_{ss} \beta_{s2} N} \right) \left(\frac{\gamma_{th2}-y}{\alpha_2 - \alpha_1 \gamma_{th2} + \alpha_1 y} \right) - \frac{\sigma^2}{\beta_{12} \theta_{P_H} k_{P_H}} y}}_I \\ &\hspace{15em} (51) \end{aligned}$$

Since D_2 assume low rate values, and $\alpha_2 > \alpha_1$ due to implementation of NOMA, we have $\alpha_2 \gg \alpha_1 \gamma_{th2}$, thus, the integral in I can be approximated as

$$\frac{e^{\frac{-\gamma_{th2}\sigma^2}{P_t\beta_{ss}\beta_{s2}N(\alpha_2-\alpha_1\gamma_{th2})}}\sigma^2}{\beta_{12}\theta_{P_H}k_{P_H}} \times \int_0^{\gamma_{th2}} e^{y\left(\frac{\sigma^2}{P_tN\beta_{ss}\beta_{s2}(\alpha_2-\alpha_1\gamma_{th2})} - \frac{\sigma^2}{\beta_{12}\theta_{P_H}k_{P_H}}\right)} dy, \quad (52)$$

whose solution can be found trivially. Substituting the solution of (52) in (51) we obtain

$$I \approx 1 - e^{\frac{\gamma_{th2}\sigma^2}{\theta_{P_H}k_{P_H}\beta_{12}}} - \frac{e^{\frac{-\gamma_{th2}\sigma^2}{P_t\beta_{ss}\beta_{s2}N(\alpha_2-\alpha_1\gamma_{th2})}}\sigma^2}{\beta_{12}\theta_{P_H}k_{P_H}} \times \left(\frac{e^{\frac{\gamma_{th2}\sigma^2}{P_t\beta_{ss}\beta_{s2}N(\alpha_2-\alpha_1\gamma_{th2})} - \frac{\gamma_{th2}\sigma^2}{\beta_{12}\theta_{P_H}k_{P_H}}} - 1}{\frac{\sigma^2}{P_t\beta_{ss}\beta_{s2}N(\alpha_2-\alpha_1\gamma_{th2})} - \frac{\sigma^2}{\beta_{12}\theta_{P_H}k_{P_H}}} \right), \quad (53)$$

utilizing the analytical results derived in Appendix B and utilizing (53), (31) is obtained and this complete the proof.

REFERENCES

- [1] M. Zeng, W. Hao, O. A. Dobre, and Z. Ding, "Cooperative noma: state of the art, key techniques, and open challenges," *IEEE Network*, vol. 34, no. 5, pp. 205–211, 2020.
- [2] W. Jiang, B. Han, M. A. Habibi, and H. D. Schotten, "The road towards 6g: A comprehensive survey," *IEEE Open Journal of the Communications Society*, vol. 2, pp. 334–366, 2021.
- [3] N. H. Mahmood, H. Alves, O. A. López, M. Shehab, D. P. M. Osorio, and M. Latva-Aho, "Six key features of machine type communication in 6g," in *2020 2nd 6G Wireless Summit (6G SUMMIT)*, 2020, pp. 1–5.
- [4] Z. Ding, M. Peng, and H. V. Poor, "Cooperative non-orthogonal multiple access in 5g systems," *IEEE Communications Letters*, vol. 19, no. 8, pp. 1462–1465, 2015.
- [5] X. Yue, Y. Liu, S. Kang, A. Nallanathan, and Z. Ding, "Exploiting full/half-duplex user relaying in noma systems," *IEEE Transactions on Communications*, vol. 66, no. 2, pp. 560–575, 2018.
- [6] Z. Zhang, Z. Ma, M. Xiao, Z. Ding, and P. Fan, "Full-duplex device-to-device-aided cooperative nonorthogonal multiple access," *IEEE Transactions on Vehicular Technology*, vol. 66, no. 5, pp. 4467–4471, 2016.
- [7] N. Ashraf, S. A. Sheikh, S. A. Khan, I. Shayea, and M. Jalal, "Simultaneous wireless information and power transfer with cooperative relaying for next-generation wireless networks: A review," *IEEE Access*, vol. 9, pp. 71 482–71 504, 2021.
- [8] C. Liu, L. Zhang, Z. Chen, and S. Li, "Outage probability analysis in downlink swipt-assisted cooperative noma systems," *Journal of Communications and Information Networks*, vol. 7, no. 1, pp. 72–87, 2022.
- [9] Z. Liu, Y. Ye, G. Lu, and R. Q. Hu, "System outage performance of swipt enabled full-duplex two-way relaying with residual hardware impairments and self-interference," *IEEE Systems Journal*, 2022.

- [10] T.-N. Tran, T. P. Vo, P. Fazio, and M. Voznak, "Swipt model adopting a ps framework to aid iot networks inspired by the emerging cooperative noma technique," *IEEE Access*, vol. 9, pp. 61 489–61 512, 2021.
- [11] T. N. Do and B. An, "Optimal sum-throughput analysis for downlink cooperative swipt noma systems," in *2018 2nd International Conference on Recent Advances in Signal Processing, Telecommunications Computing (SigTelCom)*, 2018, pp. 85–90.
- [12] W. Wu, X. Yin, P. Deng, T. Guo, and B. Wang, "Transceiver design for downlink swipt noma systems with cooperative full-duplex relaying," *IEEE Access*, vol. 7, pp. 33 464–33 472, 2019.
- [13] Y. Cheng, K. H. Li, Y. Liu, K. C. Teh, and H. V. Poor, "Downlink and uplink intelligent reflecting surface aided networks: Noma and oma," *IEEE Transactions on Wireless Communications*, vol. 20, no. 6, pp. 3988–4000, 2021.
- [14] A.-T. Le, N.-D. X. Ha, D.-T. Do, A. Silva, and S. Yadav, "Enabling user grouping and fixed power allocation scheme for reconfigurable intelligent surfaces-aided wireless systems," *IEEE Access*, vol. 9, pp. 92 263–92 275, 2021.
- [15] X. Yue and Y. Liu, "Performance analysis of intelligent reflecting surface assisted noma networks," *IEEE Transactions on Wireless Communications*, pp. 1–1, 2021.
- [16] D. Selimis, K. P. Peppas, G. C. Alexandropoulos, and F. I. Lazarakis, "On the performance analysis of ris-empowered communications over nakagami-m fading," *IEEE Communications Letters*, vol. 25, no. 7, pp. 2191–2195, 2021.
- [17] S. Li, L. Bariah, S. Muhaidat, A. Wang, and J. Liang, "Outage analysis of noma-enabled backscatter communications with intelligent reflecting surfaces," *IEEE Internet of Things Journal*, pp. 1–1, 2022.
- [18] A. Hemanth, K. Umamaheswari, A. C. Pogaku, D.-T. Do, and B. M. Lee, "Outage performance analysis of reconfigurable intelligent surfaces-aided noma under presence of hardware impairment," *IEEE Access*, vol. 8, pp. 212 156–212 165, 2020.
- [19] B. Tahir, S. Schwarz, and M. Rupp, "Analysis of uplink irs-assisted noma under nakagami-m fading via moments matching," *IEEE Wireless Communications Letters*, vol. 10, no. 3, pp. 624–628, 2021.
- [20] J. Zuo, Y. Liu, and N. Al-Dhahir, "Reconfigurable intelligent surface assisted cooperative non-orthogonal multiple access systems," *IEEE Transactions on Communications*, pp. 1–1, 2021.
- [21] G. Zhang, X. Gu, W. Duan, M. Wen, J. Choi, F. Gao, and P.-H. Ho, "Hybrid time-switching and power-splitting eh relaying for ris-noma downlink," *IEEE Transactions on Cognitive Communications and Networking*, pp. 1–1, 2022.
- [22] Q. Liu, M. Lu, N. Li, M. Li, F. Li, and Z. Zhang, "Joint beamforming and power splitting optimization for ris-assited cooperative swipt noma systems," in *2022 IEEE Wireless Communications and Networking Conference (WCNC)*, 2022, pp. 351–356.
- [23] M. Elhattab, M. A. Arfaoui, C. Assi, and A. Ghayeb, "Reconfigurable intelligent surface enabled full-duplex/half-duplex cooperative non-orthogonal multiple access," *IEEE Transactions on Wireless Communications*, vol. 21, no. 5, pp. 3349–3364, 2021.
- [24] D. Wan, M. Wen, F. Ji, Y. Liu, and Y. Huang, "Cooperative noma systems with partial channel state information over nakagami-m fading channels," *IEEE Transactions on Communications*, vol. 66, no. 3, pp. 947–958, 2017.
- [25] L. Wei, R. Q. Hu, Y. Qian, and G. Wu, "Enable device-to-device communications underlying cellular networks: challenges and research aspects," *IEEE Communications Magazine*, vol. 52, no. 6, pp. 90–96, 2014.
- [26] Y. Alsaba, C. Y. Leow, and S. K. A. Rahim, "Full-duplex cooperative non-orthogonal multiple access with beamforming and energy harvesting," *IEEE Access*, vol. 6, pp. 19 726–19 738, 2018.
- [27] H. Huang and M. Zhu, "Energy efficiency maximization design for full-duplex cooperative noma systems with swipt," *IEEE Access*, vol. 7, pp. 20 442–20 451, 2019.
- [28] Q. Y. Liao and C. Y. Leow, "Cooperative noma system with virtual full duplex user relaying," *IEEE Access*, vol. 7, pp. 2502–2511, 2018.

- [29] K. M. Rabie, A. Salem, E. Alsusa, and M.-S. Alouini, "Energy-harvesting in cooperative af relaying networks over log-normal fading channels," in *2016 IEEE International Conference on Communications (ICC)*, 2016, pp. 1–7.
- [30] T. N. Do, G. Kaddoum, T. L. Nguyen, D. B. da Costa, and Z. J. Haas, "Multi-riis-aided wireless systems: Statistical characterization and performance analysis," *arXiv preprint arXiv:2104.01912*, 2021.
- [31] Y. Jin, R. Guo, L. Zhou, and Z. Hu, "Secure beamforming for irs-assisted nonlinear swipt systems with full-duplex user," *IEEE Communications Letters*, 2022.
- [32] X. Yue, Y. Liu, S. Kang, A. Nallanathan, and Z. Ding, "Outage performance of full/half-duplex user relaying in noma systems," in *2017 IEEE International Conference on Communications (ICC)*, 2017, pp. 1–6.
- [33] E. Boshkovska, D. W. K. Ng, N. Zlatanov, and R. Schober, "Practical non-linear energy harvesting model and resource allocation for swipt systems," *IEEE Communications Letters*, vol. 19, no. 12, pp. 2082–2085, 2015.
- [34] X. Liang, X. Gong, Y. Wu, D. W. K. Ng, and T. Hong, "Analysis of outage probabilities for cooperative noma users with imperfect csi," in *2018 IEEE 4th Information Technology and Mechatronics Engineering Conference (ITOEC)*, 2018, pp. 1617–1623.
- [35] B. Tahir, S. Schwarz, and M. Rupp, "Outage analysis of uplink irs-assisted noma under elements splitting," in *2021 IEEE 93rd Vehicular Technology Conference (VTC2021-Spring)*. IEEE, 2021, pp. 1–5.
- [36] A. Papoulis and H. Saunders, "Probability, random variables and stochastic processes," 1989.
- [37] I. S. Gradshteyn and I. M. Ryzhik, *Table of integrals, series, and products*. Academic press, 2014.
- [38] M. Abramowitz and I. Stegun, *Handbook of Mathematical Functions with Formulas, Graphs, and Mathematical Tables*, ser. Applied mathematics series. U.S. Government Printing Office, 1972. [Online]. Available: <https://books.google.com.br/books?id=Cxsty7Np9sUC>
- [39] Z. Zhu, M. Ma, G. Sun, W. Hao, P. Liu, Z. Chu, and I. Lee, "Secrecy rate optimization in nonlinear energy harvesting model-based mmwave iot systems with swipt," *IEEE Systems Journal*, pp. 1–11, 2022.
- [40] S. Gao, K. Xiong, R. Jiang, L. Zhou, and H. Tang, "Outage performance of wireless-powered swipt networks with non-linear eh model in nakagami-m fading," in *2018 14th IEEE International Conference on Signal Processing (ICSP)*, 2018, pp. 668–671.